Impact of ice sheet meltwater fluxes on the climate evolution at the onset of the Last Interglacial

H. Goelzer[1]*, P. Huybrechts[1], Marie-France Loutre[2], Thierry Fichefet[2]

[1]Earth System Sciences & Departement Geografie, Vrije Universiteit Brussel, Brussels, Belgium

[2]Université catholique de Louvain, Earth and Life Institute, Georges Lemaître Centre for Earth and Climate Research (TECLIM), Louvain-la-Neuve, Belgium

*now at: Institute for Marine and Atmospheric research Utrecht, Utrecht University, the Netherlands

Correspondence to: H. Goelzer (heiko.goelzer@vub.ac.be)

Abstract

Large climate perturbations occurred during the transition between the penultimate glacial period and the Last Interglacial (Termination II), when the ice sheets retreated from their glacial configuration. Here we investigate the impact of ice sheet changes and associated freshwater fluxes on the climate evolution at the onset of the Last Interglacial. The period from 135 to 120 kyr BP is simulated with the Earth system model of intermediate complexity LOVECLIM v.1.3 with prescribed evolution of the Antarctic ice sheet, the Greenland ice sheet and the other Northern Hemisphere ice sheets. Variations in meltwater fluxes from the Northern Hemisphere ice sheets lead to North Atlantic temperature changes and modifications of the strength of the Atlantic meridional overturning circulation. By means of the interhemispheric see-saw effect, variations in the Atlantic meridional overturning circulation also give rise to temperature changes in the Southern Hemisphere, which are modulated by the direct impact of Antarctic meltwater fluxes into the Southern Ocean. Freshwater fluxes from the melting Antarctic ice sheet lead to a millennial time scale oceanic cold event in the

Southern Ocean with expanded sea ice as evidenced in some ocean sediment cores, which may be used to constrain the timing of ice sheet retreat.

1 Introduction

Understanding the climate and ice sheet evolution during past warm periods in the history of the Earth may provide important insights for projections of future climate and sea-level changes. The growing amount of paleo-reconstructions for the Last Interglacial period (e.g. Govin et al., 2012; Capron et al., 2014) in combination with improved model simulations of this most recent warm period (e.g. Bakker et al., 2013; Lunt et al., 2013, Langebroek and Nisancioglu, 2014; Loutre et al., 2014) make it an interesting target for studying the coupled climate-ice sheet system.

According to reconstructions, the Last Interglacial (LIG, from ~130-115 kyr BP) was characterised by a global annual mean surface temperature of up to 2° C above the pre-industrial (e.g. Turney and Jones, 2010; Capron et al., 2014) and a sea-level high stand of 6-9 m above the present day (Kopp et al., 2009; Dutton and Lambeck, 2012). As the penultimate glacial maximum was at least as severe as the Last Glacial Maximum (LGM) in both hemispheres (EPICA community members, 2004; Svendsen et al., 2004), this implies a large amplitude glacial-interglacial transition in terms of temperature and ice sheet configuration. At the onset of the LIG, a rapid warming of ~10°C from the preceding cold state is recorded in deep Antarctic ice cores (Masson-Delmotte et al., 2011) to have occurred between ~135 kyr BP and 130 kyr BP. Current ice core records from the Greenland ice sheet (GrIS) do not extend long enough back in time to cover the entire penultimate deglaciation and associated warming (NEEM community members, 2013), but a similar timing and magnitude of warming compared to the Antarctic can be reconstructed for sea surface temperatures off the West European margin (Sanchez Goni et al., 2012). The warming is closely related with an ice sheet retreat in both hemispheres. Despite large uncertainties in reconstructions, the global sea-level stand at 135 kyr BP of as low as -80 m (Grant et al., 2012) is indicative of the large amount of freshwater that entered the ocean in the form of meltwater from the retreating ice sheets over a relatively short period. Aside from determining the amplitude of sea-level changes, which is the focus of many studies (e.g. Robinson et al., 2011; Stone et al., 2013), the associated climate impacts and possible feedbacks on the ice sheet evolution of this

freshwater forcing are an important element for a process understanding of the coupled climate-ice sheet changes at that time.

A climatic mechanism that is thought to be directly related to changes in the NH ice sheet freshwater fluxes (FWF) is the interhemispheric see-saw effect (Stocker, 1998) that links SH warming to a weakening of the Atlantic meridional overturning circulation (AMOC). If the see-saw effect was active during the onset of the LIG, NH ice sheet melting during Termination II would have been the cause for a substantial AMOC weakening and NH cooling, while reduced interhemispheric heat transport would have caused a gradual SH warming (Stocker and Johnson 2003). The see-saw mechanism was evoked to explain part of the peak Antarctic warming during the LIG (e.g. Holden et al., 2010; Marino et al., 2015), even though some Southern Ocean (SO) warming was shown by Langebroek and Nisancioglu (2014) to be possible with orbital forcing alone (without NH freshwater forcing). The see-saw mechanism has been speculated to have caused increased Antarctic ice shelf melting and West Antarctic ice sheet (WAIS) retreat (Duplessy et al., 2007). The retreat of the WAIS, which is believed to have been grounded at the edge of the continental shelf during the penultimate glaciation, generated a large anomalous flux of freshwater into the SO. Such freshwater forcing could have had a substantial influence on the SO configuration in terms of sea ice extent and ocean circulation as shown in model experiments for the last deglaciation (Menviel et al., 2011), for future global warming scenarios (Swingedouw et al., 2008) and for the present day (Bintanja et al., 2013). The impact of increased Antarctic FWF is thought to consist of a surface ocean freshening, stratification of the surface ocean and cooling, in turn promoting sea ice growth (e.g. Bintanja et al., 2013) and reduced Antarctic Bottom Water (AABW) formation (Menviel et al., 2011). Recently, Golledge et al. (2014) suggested that such a mechanism might also have provided a feedback on Antarctic ice sheet (AIS) retreat for meltwater pulse 1A during the last glacial-interglacial transition (Termination I), by promoting warming of mid-depth ocean waters that provide additional heat for melting ice shelves.

In the present work, we study the effect of evolving ice sheet boundary conditions on the climate, by simulating the climate evolution at the onset and over the course of the LIG with an Earth system model of intermediate complexity (EMIC). The model is forced with realistic ice sheet boundary conditions from offline simulations of ice dynamic models of the AIS and GrIS and reconstructions of the other NH ice sheets. With this study we extend the work of

Loutre et al. (2014) by additionally including dynamic ice sheet changes of the GrIS and AIS and focusing on the effect of ice sheet freshwater fluxes on the climate. The model and experimental setup are described in section 2 and 3, respectively, followed by results (Sect. 4, 5 and 6), their discussion in section 7 and conclusions (Sect. 8).

2 Model description

We use the EMIC LOVECLIM version 1.3, which includes components representing the atmosphere, the ocean and sea ice, the terrestrial biosphere and the ice sheets (cf. Figure 1). The model has been utilised in a large number of coupled climate-ice sheet studies (e.g. Driesschaert et al., 2007; Swingedouw et al., 2008; Goelzer et al., 2011; 2012a; Loutre et al., 2014) and is described in detail in Goosse et al. (2010).

In this study, the climate components are forced by time-evolving ice sheet boundary conditions, which are calculated off-line, i.e. uncoupled from the climate evolution. Our modelling approach for the ice sheets consists of a combination of reconstructed NH ice sheets (except the GrIS) based on geomorphological data (Sec. 2.1) and of standalone ice dynamic simulations of the GrIS and AIS (Sec. 2.2). In either case, the boundary conditions provide time evolving topography, ice sheet extent (albedo) and spatially and temporally variable FWF to the climate model.

2.1 Northern Hemisphere ice sheet forcing

We have little geomorphological evidence for Northern Hemisphere (NH) ice sheet evolution during Termination II since it was mostly destroyed by the re-advance leading to the LGM. Therefore, the reconstruction of NH ice sheet evolution for the period of interest is made based on information from the last deglaciation. The method was already described in some detail in Loutre et al. (2014). Nevertheless, we include a more thorough description here (Appendix A). The resulting boundary conditions used to force the climate model consist of a chronology of ice mask and surface elevation changes (Figure 2) and freshwater fluxes (Figure 3a) over the entire LIG period. Support for the derived chronology of NH ice sheet evolution and their FWF can be found in records of ice-rafted detritus (IRD) from the subpolar North Atlantic (Kandiano et al., 2004; Oppo et al., 2006). These show variability of similar signature during the deglaciation and in particular a last IRD peak at ~128 kyr BP preceding low IRD levels throughout MIS 5e.

2.2 Simulations of the Greenland and Antarctic ice sheets

For the present study, the climate components are partially forced by results from stand-alone simulations of the GrIS and AIS, which have been adapted from existing ice sheet model experiments (Huybrechts 2002). The configuration of both ice sheet models and the forcing interface follows the description in Goosse et al. (2010) with the following exceptions. Forcing for the ice sheet models is derived from scaling present-day observations of temperature and precipitation with indices based on ice core records, as often done for long-term paleo ice sheet modelling (e.g. Huybrechts, 1990; Letreguilly et al., 1991; Zweck and Huybrechts, 2005; Greve et al., 2011; Stone et al., 2013). For the GrIS the forcing record was created following Fürst et al. (2015). We combine a synthesised Greenland $\delta^{18}O$ record derived from Antarctica Dome C using a bipolar seesaw model (Barker et al., 2011) with the NEEM temperature reconstruction (NEEM community members, 2013) between 128.44 kyr BP and 120 kyr BP. The Barker $\delta^{18}O$ record is converted to a spatially uniform temperature anomaly with a constant temperature/ isotope factor as $\Delta T=2.4\ °C/‰*(\delta^{18}O+34.83)$ as in Huybrechts (2002). Positive temperature anomalies of the NEEM record are scaled by a factor 0.6 to fulfil constraints on maximal ice sheet retreat from Camp Century and Dye3 ice core locations that are assumed to have been ice covered during the LIG. This places the GrIS evolution in the range of former model estimates during that period (e.g. Robinson et al., 2011; Born and Nisancioglu, 2012; Stone et al., 2013). Such scaling is in line with recent studies (e.g. Van de Berg et al., 2013; Merz et al., 2014; Sjolte et al., 2014; Steen-Larsen et al., 2014) that put in question the high temperature of the central estimate reconstructed from the NEEM record. Precipitation rates vary percentagewise as a function of the $\delta^{18}O$ record.

The AIS forcing is derived directly from the Antarctica Dome C record (EPICA community members, 2004), following again procedures described by Huybrechts (2002). Here, precipitation changes are assumed proportional to the saturated water vapour pressure gradient relative to the temperature above the surface inversion layer. Furthermore, both ice sheet models are forced by changes in global sea-level stand based on the benthic deep-sea record of Lisiecki and Raymo (2005) for the GrIS and on a more recent sea-level reconstruction using Red Sea data (Grant et al., 2012) for the AIS, where the sea-level changes are the dominant forcing. The chronology of the Red Sea record is expected to be more accurate since new dating techniques are applied (Grant et al., 2012). The impact of using another sea-level record for the GrIS simulation over the LIG is small, because of the

largely land-based character of the ice sheet during that period. The AIS model is run at a horizontal resolution of 20 x 20 km instead of 10 km x 10 km (as in the standard LOVECLIM configuration and for the GrIS model) due to computational constraints for the relatively long duration of the LIG simulation.

To embed the dynamic GrIS simulation in the other NH boundary conditions, the geometric evolution of the GrIS overrides prescribed changes where Greenland ice is present. In that case, the prescribed ice sheet evolution and associated FWF are not limited by the present-day configuration of the GrIS as in Loutre et al. (2014). With dynamic GrIS and AIS evolution, their calculated FWF (Figure 3b) replace the background freshwater flux from runoff over land calculated by the land model. The ice sheet evolution is illustrated in Figure 2 for the modelled GrIS embedded in the NH reconstruction (top) and for the modelled AIS (bottom).

In our setup, the combined sea-level contributions from Antarctica and the NH (including Greenland) fall within the 67% confidence interval of probabilistic sea-level reconstructions (Kopp et al., 2009) for the first peak in sea-level contributions and the following period (~124-120 kyr BP). For both hemispheres, the final 20 m rise in sea-level at the onset of the LIG is however steeper and occurs 1~2 kyr earlier as compared to the reconstructions. When assuming a maximum contribution from glaciers (0.42±0.11) and an additional estimate for thermal expansion of the ocean (0.4±0.3) as given by Masson-Delmotte et al. (2013), the assumed ice sheet evolution in our setup reproduces well the average sea-level contribution between 125 and 120 kyr BP from the best estimate of Kopp et al. (2009), but it does not represent the multi-peak structure of global sea-level contribution during the LIG as suggested by Kopp et al. (2009, 2013). More details about the ice sheet and sea-level evolution can be found in a companion paper (Goelzer et al., 2016) that specifically deals with the sea-level contribution of the ice sheets during the LIG in a fully coupled model set-up.

2.3 Initialisation

The goal of our initialisation technique is to prepare a climate model state for the transient simulations starting at 135 kyr BP that exhibits a minimal coupling drift. Both the GrIS and AIS models are integrated over the preceding glacial cycles and the entire LIG in stand-alone mode. The climate model is then initialized to a steady state with ice sheet boundary conditions, greenhouse gas forcing and orbital parameters for the time of coupling (135 kyr BP). In this way, when LOVECLIM is integrated forward in time for transient experiments,

the climate component is already relaxed to the ice sheet boundary conditions and exhibits a minimal model drift in unforced control experiments (not shown).

3 Experimental setup

All simulations are forced by time-dependent changes in greenhouse gas (GHG) concentrations and insolation running from 135 kyr BP until 120 kyr BP (Figure 4). The radiative forcing associated with the reconstructed GHG levels (Petit et al., 1999; Pépin et al., 2001; Raynaud et al., 2005; Loulergue et al., 2008; Spahni et al., 2005) is below preindustrial values for most of this period and barely exceeds it at ~128 kyr BP. The changes in the distribution of insolation received by the Earth are dynamically computed from the changes in the orbital configuration (Berger, 1978) and represent the governing NH forcing during peak LIG conditions aside from evolving ice sheet boundary conditions. In the following, we will compare results of the reference experiment with all ice sheet boundary conditions evolving in time (Reference) to experiments in which the ice sheet boundary conditions are partially fixed to the pre-industrial configuration (Table 1). To disentangle the effects of the individual ice sheets, the experiments noGfwf (suppressed GrIS freshwater fluxes) and noAGfwf (suppressed FWF from both AIS and GrIS) are complemented by two predecessor experiments with fixed AIS and GrIS and evolving NH boundary conditions (noAG), as well as a climate experiment forced by insolation and GHG changes only with all ice sheet boundary conditions fixed (noIS). The latter two experiments correspond to the allLR and IGonly experiments from Loutre et al. (2014).

4 Effect of GrIS and AIS on the temperature evolution at the onset of the LIG

As shown by Loutre et al. (2014), including the forcing from the NH ice sheets in terms of configuration and FWF is crucial to simulate the onset of the LIG temperature increase and its amplitude variations with LOVECLIM v.1.3 more in line with proxy records. This helps to partially overcome problems of EMICs (and general circulation models) to simulate the strong temperature contrasts inferred from proxy reconstructions (Bakker et al., 2013; Lunt et al., 2013). The increased amplitude of temperature changes in simulations including NH ice sheet boundary conditions is due to albedo and elevation changes in addition to the larger effect of the implied freshwater forcing from the NH ice sheets (Loutre et al., 2014). Here, the

Loutre et al. (2014) experiments are complemented with runs that additionally include changes in ice sheet configuration and FWF from the GrIS and AIS. We first discuss the effect of including these additional ice sheet boundary conditions. A specific focus on the FWF follows in section 5.

The temperature evolution (Figure 5) before 127 kyr BP is in both hemispheres strongly influenced by the ice sheet boundary conditions and in particular by the freshwater forcing from the ice sheets. The experiments including FWF from the NH ice sheets (Reference and noAG) clearly show temperature variations on the multi-millennial time scale in both hemispheres following variations in ice sheet freshwater input (cf. Figure 3). Differences in the temperature evolution between noAG and the reference experiment are small in the NH, where the additional freshwater flux from Greenland is small compared to the other sources. In the SH, by contrast, a large perturbation arises around 130 kyr BP, when FWF from the AIS peak. Global mean and hemispheric mean temperatures are similar in all runs after ~127 kyr BP, when the ice sheets have largely reached their interglacial configuration and their FWF are similar. An exception is the GrIS, which is retreating until ~120 kyr BP but accounts for only a small FWF contribution. The similarity of the results in the runs after ~127 kyr BP implies that the temporal memory of the response to ice sheet changes in the system is limited to the multi-centennial time scale, at least for the surface climate. The location of largest freshwater induced temperature variations in the NH is the North Atlantic between 40° N and 80° N. Here changes in the AMOC are the cause for a perturbation of the northward oceanic heat transport and temperature changes which are further amplified by sea ice-albedo and insulation feedbacks. Greenland experiences maximum warming in the reference experiment around 125 kyr BP of up to 2.7°C in the annual mean compared to the pre-industrial over remaining ice covered central Greenland. Here, the temperature evolution is largely similar to the experiment with GrIS changes not accounted for (noAG), which exhibits a maximum warming of 2.4°C (Loutre et al., 2014). However, the summer warming reaches up to 10°C at the northern margin and even up to 14°C over southern margins over a then ice-free tundra (not shown). These strong warming trends in the ice sheet periphery are due to a combination of elevation changes and local albedo changes, confined to the immediate region of ice sheet lowering and retreat. In the SH, the largest temperature perturbations linked to both NH and SH freshwater fluxes occur in the SO. The largest warming over the ice sheet itself is simulated over the WAIS and is mainly a consequence of the local elevation changes as the ice sheet retreats. However, mainly due to the marine based character of the WAIS, albedo

changes are much more limited compared to Greenland as the retreating ice sheet surface is mostly replaced by sea ice. Modelled temperature changes over the East Antarctic ice sheet (EAIS) have been compared to temperature reconstructions for four ice core locations (Figure 6). The reference experiment shows a more pronounced warming between 135 and 129.5 kyr BP compared to the experiments excluding Antarctic ice sheet changes (noAG and noIS). While the modelled warming still appears to be underestimated and delayed compared to the reconstructions, the reference simulation clearly improves the representation of the EAIS temperature evolution compared to experiments with fixed Antarctic boundary conditions.

5 Role of ice sheet meltwater fluxes

To study the role of the different freshwater contributions from the ice sheets in more detail and evaluate their importance for the climate evolution, we compare additional simulations where FWF from the GrIS and AIS are partially suppressed relative to the reference experiment (Figure 7). The ice sheet configuration (topography and albedo) remains unchanged in these experiments. The effect of AIS FWF can therefore be evaluated as the difference between noGfwf and noAGfwf, whereas the effect of GrIS FWF becomes apparent from comparing the reference simulation with noGfwf. The AIS FWF (Figure 7f) leads to considerable changes in the Southern Hemisphere, but has very little impact on the NH temperature evolution (cf. Figure 5b). Conversely, variations in the NH (Figure 7a) and GrIS freshwater forcing on millennial time-scales imply temperature changes in the SH on a background of general LIG warming.

Differences between the experiments in the AMOC evolution (Figure 7b) are largely explained by whether FWF from the NH ice sheets and the GrIS are included or not. Here, AMOC strength is calculated as the maximum value of the meridional overturning stream function below the Ekman layer in the Atlantic Ocean between 45° and 65° N. The effect of the FWF from the GrIS (cf. Reference and noGfwf in Figure 7b) is limited compared to the large impact of the general NH ice sheet forcing and consists of an additional weakening of the AMOC. It is most pronounced during periods of AMOC recovery and after 130 kyr BP, when melting of the GrIS beyond its present day configuration sets in. Note that the simulated evolution of AMOC strength in the reference experiment is in good agreement with paleo evidence based on $\delta^{13}C$ data (Bauch et al., 2012) and in particular with a recent reconstruction based on chemical water tracers (Böhm et al., 2015). The timing of Heinrich Stadial 11 (~132

kyr BP) and the variations in AMOC strength after that are well captured by our reference simulation, which gives independent credibility to our NH ice sheet reconstructions.

The evolution of NH sea ice area (Figure 7c) generally shows maxima at times of AMOC minima and vice versa and is closely linked to NH surface temperature variations (cf. Figure 5b) by modifying the heat exchange between ocean and atmosphere. The largest sea ice area between 135 and 130 kyr BP is simulated in the reference experiment, which also exhibits the lowest AMOC strength of all experiments.

The situation in the SH is more complex as surface temperature and sea ice evolution are influenced both by freshwater forcing from the AIS as by the FWF in the NH. The AMOC variability gives rise to changes in the SH through the so-called interhemispheric see-saw effect (Stocker 1998). The SH begins to warm as the NH cools due to modified oceanic heat transport across the equator. Minima in SH temperature (cf. Figure 5c) and maxima in SH sea ice area (Figure 7d) are therefore associated with maxima in AMOC strength. The additional effect of including GrIS freshwater forcing is consequently also felt in a warmer SH with less sea ice formation. However, the influence of GrIS freshwater fluxes and consequential AMOC variations on the SH temperature appears to be mostly limited to the beginning of the experiment between ~135 and 131 kyr BP. It could be speculated that this is related to the larger extent of the SH sea ice in a colder climate, making the system more sensitive due to an increased potential for sea ice-albedo and insulation feedbacks. We also note that modelled periods of increased NH freshwater fluxes, reduced AMOC strength and higher SH temperatures are roughly in phase with periods of steeper increase in GHG concentrations (cf. Figure 4b), in line with evidence from marine sediment proxies that indicate that CO_2 concentration rose most rapidly when North Atlantic Deep Water shoaled (Ahn and Brook, 2008). Since GHGs and NH freshwater fluxes are (independently) prescribed in our experiments, the described in-phase relationship lends further credibility to our NH ice sheet reconstruction.

The FWF from AIS melting (Figure 7f) increases the SO sea ice area (Figure 7d) by freshening and stratifying the upper ocean waters, which in turn leads to lower surface temperatures. In our experiments, the increased freshwater flux from the retreating AIS (cf. noGfwf versus noAGfwf) between 131 and 129 kyr BP is in phase with a period of transient AMOC strengthening (Figure 7b), which leads to a combined effect of surface cooling and sea ice expansion in the SO.

313 The formation of AABW is strongly controlled by salinity and sea ice area (and therefore
314 temperature) of the polar surface waters and hence by both Antarctic and indirectly by NH
315 freshwater fluxes. Here, the strength of AABW formation is calculated as the minimum value
316 of the global meridional overturning stream function below the Ekman layer south of 60° S.
317 The AABW formation (Figure 7e) is stronger for saltier and colder surface conditions and
318 therefore strongest in case noAGfwf, where FWF are suppressed from the AIS (saltier) and
319 the GrIS (colder). For a similar Antarctic freshwater forcing, the AABW formation is stronger
320 for a larger SH sea ice area. Including Antarctic FWF leads to a generally weaker AABW
321 formation as surface waters become fresher (cf. noGfwf versus noAGfwf). These
322 relationships imply also that a stronger decrease in AABW formation, associated with
323 decreased CO_2 uptake by the ocean can be found for periods of steeper increase in prescribed
324 radiative forcing. Again, this appears to support consistency in timing between prescribed
325 radiative and NH ice sheet forcing in our modelling.

326

327 ## 6 Temperature evolution in the Southern Hemisphere

328 Millennial scale sea-surface temperature variations in the SH induced by NH freshwater
329 fluxes are the strongest in the SO, where anomalies can be amplified by sea ice-albedo and
330 insulation feedbacks. This is also the region that experiences the largest temperature change
331 due to FWF from the AIS itself (not shown).

332 In order to study the effect of Antarctic FWF in more detail, we also analysed the oceanic
333 temperature evolution south of 63°S (Figure 8). The effect of the AIS freshwater flux in the
334 reference experiment (compare noAGfwf with reference) becomes visible in the sea surface
335 temperature after 132 kyr BP (Figure 8a) as a cooling due to stratification and sea ice
336 expansion (Figure 8c). At the same time, the subsurface ocean warms (Figure 8b) as heat is
337 trapped under the stratified surface waters and expanding sea ice area. When the FWF decline
338 towards the end of the AIS retreat around 128 kyr BP, sea ice retreats again and the heat is
339 released to the atmosphere, where it generates an overshoot in SST compared to the
340 experiment with constant Antarctic freshwater fluxes (noAGfwf). The largest effect of this
341 heat buffering is found in winter in regions of strongest warming in the Bellingshausen Sea
342 and off the Gunnerus ridge adjacent to Dronning Maud Land. The maximum sea-ice extent in
343 the SH (Figure 8c) occurs at the time of largest surface cooling at 129.5 kyr BP. This
344 freshwater induced surface cooling at the onset of the LIG appears to be superficial and

relatively short lived and of clearly different signature compared to e.g. the Antarctic cold reversal during the last deglaciation. The cooling event is indeed not recorded in our modelled temperature evolution over central East Antarctica, in line with a lack of its signature in Antarctic ice core records for that time period (Petit et al., 1999, EPICA community members, 2004). A sea ice expansion during Termination II together with an *oceanic* cold reversal around 129.5 kyr BP (Figure 8c) is however recorded in some deep-sea sediment cores, where the composition of planktonic diatoms suggests meltwater as the primary cause (Bianchi and Gersonde, 2002; Cortese and Abelmann, 2002).

As a further consequence, the timing of maximum annual mean surface air temperature (defined as MWT for Maximum Warmth Timing; Bakker et al., 2013) in the SO differs by several thousand years between experiments (Figure 9). Including Antarctic FWF leads to an earlier MWT (by up to 2 kyr) in large parts of the SO south of 60°S and in the central and eastern parts of the Atlantic sector of the SO up to 40°S (Figure 9d). Conversely, a later MWT (by up to 3 kyr) is found in the Indian and Pacific sectors of the SO north of 60°S when Antarctic FWF is accounted for (Figure 9d). In the reference experiment (Figure 9a) and noGfwf (Figure 9b), the MWT lies relatively homogeneously between -129 kyr and -128 kyr for the entire SO south of 45°S and coincides with the overshoot in SST after the peak input of Antarctic FWF. The observed changes of the MWT in the SO due to the additional Antarctic freshwater input can therefore in either way be understood as a shift towards the time when heat from the mid-depth ocean buffer is released to the surface.

7 Discussion

Despite remaining uncertainties in the timing of ice sheet retreat during Termination II, we find several lines of evidence in support of our ice sheet reconstructions and the associated climatic signatures. The NH ice sheet reconstruction shows some similarity with the IRD signal recorded in North Atlantic sediment cores (Kandiano et al., 2004; Oppo et al., 2006), while the simulated evolution of the AMOC strength (Figure 7a) is in good agreement with a recent reconstruction based on chemical water tracers (Böhm et al., 2015). The combination of NH and SH sourced freshwater forcing variations produces a stronger decrease in AABW formation, associated with decreased CO_2 uptake by the ocean for periods of steeper increase in prescribed radiative forcing, in line with evidence from marine sediment proxies that

376 indicate that CO_2 concentration rose most rapidly when North Atlantic Deep Water shoaled
377 (Ahn and Brook, 2008).

378 Our modelling results furthermore suggest that the major AIS retreat from its glacial
379 configuration could be constrained by an oceanic cold event recorded in several SO sediment
380 cores around Antarctica (Bianchi and Gersonde, 2002; Cortese and Abelmann, 2002). As a
381 schematic sensitivity test to uncertainties in the overall glacial AIS volume, we have
382 performed one more experiment identical to the reference experiment except for Antarctic
383 FWF scaled to 50% of their reference value. The resulting magnitude of the SO cold event
384 and overshoot is lower but exhibits the same timing and spatial expression as in the reference
385 case. The described mechanisms and effects can therefore be considered robust to differences
386 in the assumed glacial AIS volume. Notably, the improved representation of the central East
387 Antarctic temperature evolution in the model when including Antarctic ice sheet changes
388 (Figure 6) is largely independent of the chosen freshwater forcing. This implies that changes
389 in the geometry of the ice sheet and modified atmospheric circulation patterns are the cause
390 for the stronger simulated temperature contrast.

391 The GrIS is generally assumed to have remained largely intact during the LIG (e.g. Robinson
392 et al., 2011; Colville et al., 2011; Stone et al., 2013; NEEM community members, 2013) and
393 indirect evidence of its freshwater contribution may be difficult to find due to the low
394 amplitude compared to the other Northern Hemisphere ice sheets. However, recent ice core
395 reconstructions of the temperature evolution at the NEEM ice core site (NEEM community
396 members, 2013) point to a late retreat with a peak sea-level contribution close to 120 kyr BP.
397 This is the case even if the amplitude of the central estimate of the reconstructed temperature
398 anomaly may be debated (e.g. Van de Berg et al., 2013; Merz et al., 2014; Sjolte et al., 2014;
399 Steen-Larsen et al., 2014). The GrIS can be assumed to lose mass approximately as long as
400 the climatic temperature anomaly above the ice sheet remains above zero. Based on the
401 NEEM record, which has been used as forcing time series in our stand-alone GrIS
402 experiment, FWF from the GrIS peak at ~125 kyr BP, but remains elevated until around 120
403 kyr BP above the steady state background flux of an ice sheet in equilibrium with the climate.
404 The additional FWF from melting of the GrIS results in relatively low temperatures over
405 Southeast Greenland in response to a weakening of the AMOC (not shown). The interaction
406 between GrIS meltwater fluxes and oceanic circulation hence give rise to a negative feedback
407 on ice sheet retreat. This aspect could play an important role for the stability of the southern

dome of the ice sheet and should be examined further with fully coupled climate-ice sheet simulations.

In general, the NH freshwater forcing leads to variations in the strength of the AMOC and North Atlantic cooling and additionally through the bipolar see-saw effect, to temperature changes in the SH. The only moment mid-depth ocean temperatures close to AIS grounding lines are above pre-industrial values in our experiments is during the oceanic cold reversal around 129.5 kyr BP, induced by anomalous FWF from the retreating AIS. During this period, SO mid-depth temperature anomalies relative to the pre-industrial reach up to 0.3 K, which could provide a positive but rather limited feedback on ice sheet retreat, similar to what has been suggested by Golledge et al. (2014) for meltwater pulse 1A during Termination I. However, the oceanic warming recorded in our model is not strong and the duration of the perturbation does not appear to be long enough for a sustained impact on the retreat of the ice sheet. Furthermore, the peak in freshwater flux appears when the ice sheet has already retreated considerably and WAIS grounding lines are located mostly on the continental shelves, more protected from the warm water build-up in the mid-depth ocean. A large-scale marine ice sheet retreat of the likely less vulnerable EAIS sectors (Mengel and Levermann, 2014) appears particularly unlikely, given the atmospheric and oceanic forcing at the time apparent in our modelling results. However, in-depth studies of these interactions require detailed coupled simulations of the entire ocean-ice sheet system.

Despite aforementioned lines of evidence in support of the reconstructed NH ice sheet evolution, a limitation to our modelling approach is the rescaling of post-LGM NH ice sheet retreat, an attempt to address the sparseness of geomorphological field evidence for Termination II. An alternative approach would be to physically model all ice sheets together in one framework (e.g. de Boer et al. 2013), although spatial and temporal resolution of the models is a limiting factor in that specific case. A rigorous modelling approach like the latter could also help to prevent possible inconsistencies when combining ice sheet reconstructions from different approaches. Nevertheless, any modelling approach will ultimately be confronted with the same problem of scarce data for model validation during that period. The exclusion of climate feedbacks on ice sheet evolution of our present one-way coupled modelling approach is a general limitation, which we have addressed in a separate study with a fully coupled model set-up (Goelzer et al., 2016).

8 Conclusion

We have presented a transient simulation of Termination II and the Last Interglacial period with realistic ice sheet boundary conditions from reconstructed Northern Hemisphere ice sheets and detailed stand-alone simulations of the Greenland and Antarctic ice sheets. Our results show that the temperature evolution at the onset of the Last Interglacial was in both hemispheres considerably influenced by meltwater fluxes from the retreating ice sheets. While Antarctic freshwater fluxes lead to strong perturbations of the Southern Ocean, Northern Hemisphere freshwater fluxes have an influence both on the Northern and Southern Hemisphere temperature evolution through the oceanic see-saw effect. The importance of additional freshwater input from the GrIS during Termination II is small compared to the much larger fluxes from the other NH ice sheets and becomes more important only later during the Interglacial when it is the only remaining ice sheet contributing freshwater fluxes to the North Atlantic. In the Southern Hemisphere, anomalous freshwater input from the AIS leads to an episode of surface freshening, increased stratification and sea ice cover and consequently reduced ocean heat loss to the atmosphere, with temporary heat build-up in the mid-depth ocean. We argue that the surface ocean cooling associated with this event may be used to constrain an early Antarctic retreat when matched with similar signatures evident in some deep-sea sediment cores from the Southern Ocean.

Our transient simulations confirm results from earlier studies that stress the importance of ice sheet boundary conditions for the climate evolution at the onset of the LIG. However, most of the freshwater induced changes remain visible for at most 1-2 kyr after cessation of the perturbations, indicative of a relative short memory of the (surface) climate system. Additional effects may arise from climate-ice sheet feedbacks not considered in the present model configuration, which should be investigated in fully-coupled experiments.

Appendix: Reconstruction of NH ice sheet forcing

A direct reconstruction of NH ice sheet evolution during Termination II based on geomorphological data is not possible, due to the scarcity of field evidence that was mostly destroyed by the re-advancing ice sheets during the last glacial period. Therefore, a reconstruction of Termination II is made by remapping the much better constrained post-LGM retreat.

Post-LGM ice extent

The evolution of the northern hemisphere ice extent since the LGM was estimated based on published sources (Table A1) dating back to the time of the NH ice sheet studies of Zweck and Huybrechts (2003, 2005). For the large Laurentide and Eurasian ice sheets inferred ice extents are relatively well determined from geomorphological data and the reconstruction remains in good agreement with most recent sources (e.g. Hughes et al. 2016). For smaller ice sheets such as the European Alps previous modelled ice extent was used (Zweck and Huybrechts, 2005).

For ice sheets with multiple sources of data the isochrones were merged using the more recent source when conflicts occurred (e.g. Dyke et al. (2002) instead of Dyke and Prest (1987) for the Innuitian ice sheet, Svendsen et al. (1999) instead of Andersen (1981) for the LGM maximum of the Eurasian ice sheet). The more recent source was then used as a mask of maximum ice extent for more recent isochrones of all sources. The only region which experienced an advance in post LGM ice extent using this technique was the southern Cordilleran ice sheet according to the reconstruction of Clague and James (2001).

The INTCAL98 timescale of Stuiver et al. (1998) was used to convert radiocarbon dates to calendar years for the sources in Table A1. The retreat of the ice sheets between the LGM and PD was prescribed at 200 year resolution. Even for well-determined geomorphological observations uncertainties in dating and the conversion from radiocarbon to calendar years well exceed the 200 year temporal resolution used here. Figure A1 shows the deglaciation chronology reconstructed in this manner.

Post-LGM ice sheet elevations

The northern hemisphere ice sheets introduced significant changes to the surface topography of the region. As LOVECLIM1.3 has only 3 atmospheric height levels, details regarding topography are not strongly sensed. To include changes in surface topography in the model, parabolic profile ice sheets are constructed using the extents shown in Figure A1, assuming conditions of no isostatic adjustment (i.e. present day surface elevation of the Earth's surface). The basal shear stress for the parabolic profile reconstruction is chosen so that the difference in ice volume between LGM and PD corresponds to 86 m of eustatic sea level change. This value is chosen so that were isostasy accounted for an additional 24 m of ice would produce a similar elevation and contribute a total equivalent eustatic sea level change of 110 m, in keeping with the results for the Northern Hemisphere ice sheets since the LGM

of Zweck and Huybrechts (2005). Using this procedure the maximum elevation of the Laurentide ice sheet is 3000 m near present day Churchill in Hudson Bay, and the maximum elevation of the Eurasian ice sheet is 2600 m 100 km west of present day Helsinki.

Remapping post-LGM retreat to Termination II

Remapping of the post-LGM retreat to Termination II is done using a benthic $\delta^{18}O$ record (Lisiecki and Raymo, 2005), assumed as an indicator of the global ice volume. In practice, the NH ice sheet configuration for a given time (and $\delta^{18}O$ value) during Termination II is taken from a time during the post-LGM retreat when the $\delta^{18}O$ value had the same value. The LGM sea-level contribution of the NH ice sheets relative to the present day of -110 m translates into a similar magnitude for the penultimate glacial maximum (Lisiecki and Raymo, 2005). However, the method does not guarantee that the sea-level contribution of the reconstructed NH ice sheets closely follows the global ice volume curve. This is generally due to the mismatch between global ice volume and NH ice sheet reconstruction during the post-LGM period, and in part related to the unconstrained contribution of other components (AIS, thermal expansion). Due to the assumed analogy, different configurations of the Northern Hemisphere ice sheets (e.g. Obrochta et al., 2014) and different relative timing of NH and SH deglaciation between last and penultimate glaciation are not represented in these reconstructions. NH freshwater fluxes were estimated from the same method by using derived volume changes as input to a continental runoff routing model (Goelzer et al., 2012b) to identify the magnitude and location of meltwater fluxes to the ocean.

9 Acknowledgements

We acknowledge support through the Belgian Federal Science Policy Office within its Research Programme on Science for a Sustainable Development under contract SD/CS/06A (iCLIPS). Computational resources have been provided by the supercomputing facilities of the Université catholique de Louvain (CISM/UCL) and the Consortium des Equipements de Calcul Intensif en Fédération Wallonie Bruxelles (CECI) funded by the Fond de la Recherche Scientifique de Belgique (FRS-FNRS).

10 References

Ahn, J., and Brook, E.: Atmospheric CO_2 and climate on millennial time scales during the last glacial period, Science, 322, 83-85, doi: 10.1126/science.1160832 2008.

Andersen, B. G.: Late Weichselian ice sheets in Eurasia and Greenland, in: The Last Great Ice Sheets, edited by: Denton, G. H., and Hughes, T. J., Wiley Interscience, New York, 1 - 65, 1981.

Bakker, P., Stone, E. J., Charbit, S., Gröger, M., Krebs-Kanzow, U., Ritz, S. P., Varma, V., Khon, V., Lunt, D. J., Mikolajewicz, U., Prange, M., Renssen, H., Schneider, B., and Schulz, M.: Last interglacial temperature evolution – a model inter-comparison, Clim. Past., 9, 605-619, doi:10.5194/cp-9-605-2013, 2013.

Barker, S., Knorr, G., Edwards, R. L., Parrenin, F., Putnam, A. E., Skinner, L. C., Wolff, E., and Ziegler, M.: 800,000 Years of Abrupt Climate Variability, Science, 334, 347-351, doi:10.1126/science.1203580 2011.

Bauch, H. A., Kandiano, E. S., and Helmke, J. P.: Contrasting ocean changes between the subpolar and polar North Atlantic during the past 135 ka, Geophys. Res. Lett., 39, L11604, doi:10.1029/2012GL051800, 2012.

Berger, A.: Long-term variations of daily insolation and Quaternary climatic changes, Journal of Atmospheric Sciences, 35, 2362-2367, doi:10.1175/1520-0469(1978)035<2362:LTVODI>2.0.CO;2, 1978.

Bianchi, C., and Gersonde, R.: The Southern Ocean surface between Marine Isotope Stages 6 and 5d: Shape and timing of climate changes, Palaeogeography, Palaeoclimatology, Palaeoecology, 187, 151-177, doi:10.1016/S0031-0182(02)00516-3, 2002.

Bintanja, R., Van Oldenborgh, G. J., Drijfhout, S. S., Wouters, B., and Katsman, C. A.: Important role for ocean warming and increased ice-shelf melt in Antarctic sea-ice expansion, Nat. Geosci., 6, 376-379, doi:10.1038/ngeo1767, 2013.

Böhm, E., Lippold, J., Gutjahr, M., Frank, M., Blaser, P., Antz, B., Fohlmeister, J., Frank, N., Andersen, M. B., and Deininger, M.: Strong and deep Atlantic meridional overturning circulation during the last glacial cycle, Nature, 517, 73–76 doi:10.1038/nature14059, 2015.

Born, A., and Nisancioglu, K. H.: Melting of Northern Greenland during the last interglaciation, Cryosphere, 6, 1239-1250, doi:10.5194/tc-6-1239-2012, 2012.

563 Brovkin, V., Ganopolski, A., and Svirezhev, Y.: A continuous climate-vegetation
564 classification for use in climate-biosphere studies, Ecol. Model., 101, 251-261,
565 doi:10.1016/S0304-3800(97)00049-5, 1997.

566 Capron, E., Govin, A., Stone, E. J., Masson-Delmotte, V., Mulitza, S., Otto-Bliesner, B.,
567 Rasmussen, T. L., Sime, L. C., Waelbroeck, C., and Wolff, E. W.: Temporal and spatial
568 structure of multi-millennial temperature changes at high latitudes during the Last
569 Interglacial, Quat. Sci. Rev., 103, 116-133, doi:10.1016/j.quascirev.2014.08.018, 2014.

570 Clague, J. J., and James, T. S.: History and isostatic effects of the last ice sheet in southern
571 British Columbia, Quat. Sci. Rev., 21, 71-87, doi:10.1016/s0277-3791(01)00070-1, 2002.

572 Colville, E. J., Carlson, A. E., Beard, B. L., Hatfield, R. G., Stoner, J. S., Reyes, A. V., and
573 Ullman, D. J.: Sr-Nd-Pb Isotope Evidence for Ice-Sheet Presence on Southern Greenland
574 During the Last Interglacial, Science, 333, 620-623, doi:10.1126/science.1204673, 2011.

575 Cortese, G., and Abelmann, A.: Radiolarian-based paleotemperatures during the last 160 kyr
576 at ODP Site 1089 (Southern Ocean, Atlantic Sector), Palaeogeography, Palaeoclimatology,
577 Palaeoecology, 182, 259-286, doi:10.1016/S0031-0182(01)00499-0, 2002.

578 de Boer, B., van de Wal, R. S. W., Lourens, L. J., Bintanja, R., and Reerink, T. J.: A
579 continuous simulation of global ice volume over the past 1 million years with 3-D ice-sheet
580 models, Clim. Dyn., 41, 1365-1384, doi:10.1007/s00382-012-1562-2, 2013.

581 Driesschaert, E., Fichefet, T., Goosse, H., Huybrechts, P., Janssens, I., Mouchet, A.,
582 Munhoven, G., Brovkin, V., and Weber, S.: Modeling the influence of Greenland ice sheet
583 melting on the Atlantic meridional overturning circulation during the next millennia,
584 Geophys. Res. Lett., 34, 10707, doi:10.1029/2007GL029516, 2007.

585 Duplessy, J. C., Roche, D. M., and Kageyama, M.: The deep ocean during the last interglacial
586 period, Science, 316, 89-91, doi:10.1126/science.1138582, 2007.

587 Dutton, A., and Lambeck, K.: Ice Volume and Sea Level During the Last Interglacial,
588 Science, 337, 216-219, doi:10.1126/science.1205749, 2012.

589 Dyke, A. S., Andrews, J. T., Clark, P. U., England, J., Miller, G. H., Shaw, J., and Veillette, J.
590 J.: The Laurentide and Innuitian ice sheets during the Last Glacial Maximum, Quat. Sci. Rev.,
591 21, 9-31, doi:10.1016/S0277-3791(01)00095-6, 2002.

592 Dyke, A. S., and Prest, V. K.: Late Wisconsinan and Holocene history of the Laurentide Ice
593 Sheet, Géog. Phys. Quat., 41, 237 - 263, doi:10.7202/032681ar, 1987.

594 EPICA community members: Eight glacial cycles from an Antarctic ice core, Nature, 429,
595 623-628, doi:10.1038/Nature02599, 2004.

596 Fürst, J. J., Goelzer, H., and Huybrechts, P.: Ice-dynamic projections of the Greenland ice
597 sheet in response to atmospheric and oceanic warming, The Cryosphere, 9, 1039-1062,
598 doi:10.5194/tc-9-1039-2015, 2015.

599 Goelzer, H., Huybrechts, P., Loutre, M. F., Goosse, H., Fichefet, T., and Mouchet, A.: Impact
600 of Greenland and Antarctic ice sheet interactions on climate sensitivity, Clim. Dyn., 37, 1005-
601 1018, doi:10.1007/s00382-010-0885-0, 2011.

602 Goelzer, H., Huybrechts, P., Raper, S. C. B., Loutre, M. F., Goosse, H., and Fichefet, T.:
603 Millennial total sea level commitments projected with the Earth system model of intermediate
604 complexity LOVECLIM, Environ. Res. Lett., 7, doi:10.1088/1748-9326/7/4/045401, 2012a.

605 Goelzer, H., Janssens, I., Nemec, J., and Huybrechts, P.: A dynamic continental runoff
606 routing model applied to the last Northern Hemisphere deglaciation, Geosci. Model Dev., 5,
607 599-609, doi:10.5194/gmd-5-599-2012, 2012b.

608 Goelzer, H., Huybrechts, P., Loutre, M.-F., and Fichefet, T.: Last Interglacial climate and sea-
609 level evolution from a coupled ice sheet-climate model, Clim. Past. Discuss., in review,
610 doi:10.5194/cp-2015-175, 2016.

611 Golledge, N. R., Menviel, L., Carter, L., Fogwill, C. J., England, M. H., Cortese, G., and
612 Levy, R. H.: Antarctic contribution to meltwater pulse 1A from reduced Southern Ocean
613 overturning, Nature Communications, 5, doi:10.1038/ncomms6107, 2014.

614 Goosse, H., and Fichefet, T.: Importance of ice-ocean interactions for the global ocean
615 circulation: A model study, J. Geophys. Res., 104, 23337-23355, doi:10.1029/1999JC900215,
616 1999.

617 Goosse, H., Brovkin, V., Fichefet, T., Haarsma, R., Huybrechts, P., Jongma, J., Mouchet, A.,
618 Selten, F., Barriat, P.-Y., Campin, J.-M., Deleersnijder, E., Driesschaert, E., Goelzer, H.,
619 Janssens, I., Loutre, M. F., Morales Maqueda, M. A., Opsteegh, T., Mathieu, P.-P.,
620 Munhoven, G., Pettersson, E. J., Renssen, H., Roche, D. M., Schaeffer, M., Tartinville, B.,
621 Timmermann, A., and Weber, S. L.: Description of the Earth system model of intermediate

622 complexity LOVECLIM version 1.2, Geosci. Model Dev., 3, 603-633, doi:10.5194/gmd-3-
623 603-2010, 2010.

624 Govin, A., Braconnot, P., Capron, E., Cortijo, E., Duplessy, J. C., Jansen, E., Labeyrie, L.,
625 Landais, A., Marti, O., Michel, E., Mosquet, E., Risebrobakken, B., Swingedouw, D., and
626 Waelbroeck, C.: Persistent influence of ice sheet melting on high northern latitude climate
627 during the early Last Interglacial, Clim. Past., 8, 483-507, doi:10.5194/cp-8-483-2012, 2012.

628 Grant, K. M., Rohling, E. J., Bar-Matthews, M., Ayalon, A., Medina-Elizalde, M., Ramsey,
629 C. B., Satow, C., and Roberts, A. P.: Rapid coupling between ice volume and polar
630 temperature over the past 150,000 years, Nature, 1-4, doi:10.1038/nature11593, 2012.

631 Greve, R., Saito, F., and Abe-Ouchi, A.: Initial results of the SeaRISE numerical experiments
632 with the models SICOPOLIS and IcIES for the Greenland ice sheet, Ann. Glaciol., 52, 23-30,
633 doi:10.3189/172756411797252068, 2011.

634 Holden, P., Edwards, N. R., Wolff, E., Lang, N., Singarayer, J., Valdes, P., and Stocker, T.:
635 Interhemispheric coupling, the West Antarctic Ice Sheet and warm Antarctic interglacials,
636 Clim. Past., 6, 431-443, doi:10.5194/cp-6-431-2010, 2010.

637 Hughes, A. L. C., Gyllencreutz, R., Lohne, Ø. S., Mangerud, J., and Svendsen, J. I.: The last
638 Eurasian ice sheets – a chronological database and time-slice reconstruction, DATED-1,
639 Boreas, 45, 1-45, doi:10.1111/bor.12142, 2016.

640 Huybrechts, P.: A 3-D model for the Antarctic Ice Sheet: a sensitivity study on the glacial-
641 interglacial contrast, Clim. Dyn., 5, 79-92, doi:10.1007/BF00207423, 1990.

642 Huybrechts, P.: Sea-level changes at the LGM from ice-dynamic reconstructions of the
643 Greenland and Antarctic ice sheets during the glacial cycles, Quat. Sci. Rev., 21, 203-231,
644 doi:10.1016/S0277-3791(01)00082-8, 2002.

645 Kandiano, E. S., Bauch, H. A., and Müller, A.: Sea surface temperature variability in the
646 North Atlantic during the last two glacial–interglacial cycles: comparison of faunal, oxygen
647 isotopic, and Mg/Ca-derived records, Palaeogeography, Palaeoclimatology, Palaeoecology,
648 204, 145-164, doi:10.1016/S0031-0182(03)00728-4, 2004.

649 Kopp, R. E., Simons, F. J., Mitrovica, J. X., Maloof, A. C., and Oppenheimer, M.:
650 Probabilistic assessment of sea level during the last interglacial stage, Nature, 462, 863-867,
651 doi:10.1038/nature08686, 2009.

652 Kopp, R. E., Simons, F. J., Mitrovica, J. X., Maloof, A. C., and Oppenheimer, M.: A
653 probabilistic assessment of sea level variations within the last interglacial stage, Geophys. J.
654 Int., 193, 711-716, doi:10.1093/gji/ggt029, 2013.

655 Landvik, J. Y., Bondevik, S., Elverhøi, A., Fjeldskaar, W., Mangerud, J., Salvigsen, O.,
656 Siegert, M. J., Svendsen, J. I., and Vorren, T. O.: The Last Glacial Maximum of Svalbard and
657 the Barents Sea area: ice sheet extent and configuration, Quat. Sci. Rev., 17, 43-75,
658 doi:10.1016/S0277-3791(97)00066-8, 1998.

659 Langebroek, P. M., and Nisancioglu, K. H.: Simulating last interglacial climate with
660 NorESM: role of insolation and greenhouse gases in the timing of peak warmth, Clim. Past.,
661 10, 1305-1318, doi:10.5194/cp-10-1305-2014, 2014.

662 Letreguilly, A., Huybrechts, P., and Reeh, N.: Steady-state characteristics of the Greenland
663 ice sheet under different climates, J. Glaciol., 37, 149-157, 1991.

664 Lisiecki, L. E., and Raymo, M. E.: A Pliocene-Pleistocene stack of 57 globally distributed
665 benthic delta O-18 records, Paleoceanography, 20, 17, doi:10.1029/2004pa001071, 2005.

666 Loulergue, L., Schilt, A., Spahni, R., Masson-Delmotte, V., Blunier, T., Lemieux, B.,
667 Barnola, J.-M., D. Raynaud, Stocker, T. F., and Chappellaz, J.: Orbital and millennial-scale
668 features of atmospheric CH_4 over the past 800,000 years, Nature, 453, 383-386,
669 doi:10.1038/nature06950, 2008.

670 Loutre, M. F., Fichefet, T., Goosse, H., Huybrechts, P., Goelzer, H., and Capron, E.: Factors
671 controlling the last interglacial climate as simulated by LOVECLIM1.3, Clim. Past., 10,
672 1541-1565, doi:10.5194/cp-10-1541-2014, 2014.

673 Lunt, D. J., Abe-Ouchi, A., Bakker, P., Berger, A., Braconnot, P., Charbit, S., Fischer, N.,
674 Herold, N., Jungclaus, J. H., Khon, V. C., Krebs-Kanzow, U., Langebroek, P. M., Lohmann,
675 G., Nisancioglu, K., Otto-Bliesner, B., Park, W., Pfeiffer, M., Phipps, S. J., Prange, M.,
676 Rachmayani, R., Renssen, H., Rosenbloom, N., Schneider, B., Stone, E. J., Takahashi, K.,
677 Wei, W., Yin, Q., and Zhang, Z. S.: A multi-model assessment of last interglacial
678 temperatures, Clim. Past., 9, 699-717, doi:10.5194/cp-9-699-2013, 2013.

679 Mangerud, J., Astakhov, V., and Svendsen, J. I.: The extent of the Barents-Kara Ice Sheet
680 during the Last Glacial Maximum, Quat. Sci. Rev., 21, 111-119, doi:10.1016/s0277-
681 3791(01)00088-9, 2002.

682 Marino, G., Rohling, E. J., Rodriguez-Sanz, L., Grant, K. M., Heslop, D., Roberts, A. P.,
683 Stanford, J. D., and Yu, J.: Bipolar seesaw control on last interglacial sea level, Nature, 522,
684 197-201, doi:10.1038/nature14499, 2015.

685 Masson-Delmotte, V., Buiron, D., Ekaykin, A., Frezzotti, M., Gallée, H., Jouzel, J., Krinner,
686 G., Landais, A., Motoyama, H., Oerter, H., Pol, K., Pollard, D., Ritz, C., Schlosser, E., Sime,
687 L. C., Sodemann, H., Stenni, B., Uemura, R., and Vimeux, F.: A comparison of the present
688 and last interglacial periods in six Antarctic ice cores, Clim. Past., 7, 397-423,
689 doi:10.5194/cp-7-397-2011, 2011.

690 Masson-Delmotte, V., Schulz, M., Abe-Ouchi, A., Beer, J., Ganopolski, A., González Rouco,
691 J., Jansen, E., Lambeck, K., Luterbacher, J., Naish, T., Osborn, T., Otto-Bliesner, B., T.
692 Quinn, R. R., M. Rojas, X. S., and Timmermann, A.: Information from paleoclimate archives,
693 in: Climate Change 2013: The Physical Science Basis. Contribution of Working Group I to
694 the Fifth Assessment Report of the Intergovernmental Panel on Climate Change, edited by:
695 Stocker, T. F., Qin, D., Plattner, G.-K., Tignor, M., Allen, S. K., Boschung, J., Nauels, A.,
696 Xia, Y., Bex, V., and Midgley, P. M., Cambridge University Press, , Cambridge, United
697 Kingdom and New York, NY, USA, 383-464, 2013.

698 Mayewski, P., Denton, G., and Hughes, T.: Late Wisconsin Ice Sheets in North America, in:
699 The Last Great Ice Sheets, edited by: Denton, G., and Hughes, T., Wiley Interscience, New
700 York, 67-178, 1981.

701 Mengel, M., and Levermann, A.: Ice plug prevents irreversible discharge from East
702 Antarctica, Nature Climate Change, 4, 451-455, doi:10.1038/nclimate2226, 2014.

703 Menviel, L., Timmermann, A., Timm, O. E., and Mouchet, A.: Deconstructing the Last
704 Glacial termination: the role of millennial and orbital-scale forcings, Quat. Sci. Rev., 30,
705 1155-1172, doi:10.1016/j.quascirev.2011.02.005, 2011.

706 Merz, N., Born, A., Raible, C. C., Fischer, H., and Stocker, T. F.: Dependence of Eemian
707 Greenland temperature reconstructions on the ice sheet topography, Clim. Past, 10, 1221-
708 1238, doi:10.5194/cp-10-1221-2014, 2014.

709 NEEM community members: Eemian interglacial reconstructed from a Greenland folded ice
710 core, Nature, 493, 489-494, doi:10.1038/nature11789, 2013.

711 Obrochta, S. P., Crowley, T. J., Channell, J. E. T., Hodell, D. A., Baker, P. A., Seki, A., and
712 Yokoyama, Y.: Climate variability and ice-sheet dynamics during the last three glaciations,
713 Earth Planet. Sci. Lett., 406, 198-212, doi:10.1016/j.epsl.2014.09.004, 2014.

714 Oppo, D. W., McManus, J. F., and Cullen, J. L.: Evolution and demise of the Last Interglacial
715 warmth in the subpolar North Atlantic, Quat. Sci. Rev., 25, 3268-3277,
716 doi:10.1016/j.quascirev.2006.07.006, 2006.

717 Opsteegh, J. D., Haarsma, R. J., Selten, F. M., and Kattenberg, A.: ECBILT: a dynamic
718 alternative to mixed boundary conditions in ocean models, Tellus, 50, 348-367,
719 doi:10.1034/j.1600-0870.1998.t01-1-00007.x, 1998.

720 Pepin, L., Raynaud, D., Barnola, J. M., and Loutre, M. F.: Hemispheric roles of climate
721 forcings during glacial-interglacial transitions as deduced from the Vostok record and LLN-
722 2D model experiments, J. Geophys. Res. [Atmos.], 106, 31885-31892,
723 doi:10.1029/2001jd900117, 2001.

724 Petit, J.-R., Jouzel, J., Raynaud, D., Barkov, N. I., Barnola, J.-M., Basile, I., Bender, M.,
725 Chappellaz, J., Davis, M. E., Delaygue, G., Delmotte, M., Kotlyakov, V. M., Legrand, M.,
726 Lipenkov, V. Y., Lorius, C., Pepin, L., Ritz, C., Saltzman, E., and Stievenard, M.: Climate
727 and atmospheric history of the past 420,000 years from the Vostok ice core, Antarctica,
728 Nature, 399, 429-436, doi:10.1038/20859, 1999.

729 Raynaud, D., Barnola, J. M., Souchez, R., Lorrain, R., Petit, J. R., Duval, P., and Lipenkov,
730 V. Y.: Palaeoclimatology - The record for marine isotopic stage 11, Nature, 436, 39-40,
731 doi:10.1038/43639b, 2005.

732 Robinson, A., Calov, R., and Ganopolski, A.: Greenland ice sheet model parameters
733 constrained using simulations of the Eemian Interglacial, Clim. Past., 7, 381-396,
734 doi:10.5194/cp-7-381-2011, 2011.

735 Sanchez Goni, M. F., Bakker, P., Desprat, S., Carlson, A. E., Van Meerbeeck, C. J., Peyron,
736 O., Naughton, F., Fletcher, W. J., Eynaud, F., Rossignol, L., and Renssen, H.: European
737 climate optimum and enhanced Greenland melt during the Last Interglacial, Geology, 40,
738 627-630, doi:10.1130/G32908.1 2012.

739 Sjolte, J., and Hoffmann, G.: Modelling stable water isotopes in monsoon precipitation during
740 the previous interglacial, Quat. Sci. Rev., 85, 119-135, doi:10.1016/j.quascirev.2013.12.006,
741 2014.

742 Spahni, R., Chappellaz, J., Stocker, T. F., Loulerge, L., Hausammann, G., Kawamura, K.,
743 Flückiger, J., Schwander, J., Raynaud, D., Masson-Delmotte, V., and Jouzel, J.: Atmospheric
744 methane and nitrous oxide of the late Pleistocene from Antarctic ice cores, Science, 310,
745 1317-1321, doi:10.1126/science.1120132 2005.

746 Steen-Larsen, H. C., Masson-Delmotte, V., Hirabayashi, M., Winkler, R., Satow, K., Prié, F.,
747 Bayou, N., Brun, E., Cuffey, K. M., Dahl-Jensen, D., Dumont, M., Guillevic, M., Kipfstuhl,
748 S., Landais, A., Popp, T., Risi, C., Steffen, K., Stenni, B., and Sveinbjörnsdottír, A. E.: What
749 controls the isotopic composition of Greenland surface snow?, Clim. Past., 10, 377-392,
750 doi:10.5194/cp-10-377-2014, 2014.

751 Stocker, T. F.: The Seesaw Effect, Science, 282, 61-62, doi:10.1126/science.282.5386.61,
752 1998.

753 Stocker, T. F., and Johnsen, S. J.: A minimum thermodynamic model for the bipolar seesaw,
754 Paleoceanography, 18, 1087, doi:10.1029/2003PA000920, 2003.

755 Stone, E. J., Lunt, D. J., Annan, J. D., and Hargreaves, J. C.: Quantification of the Greenland
756 ice sheet contribution to Last Interglacial sea level rise, Clim. Past., 9, 621-639,
757 doi:10.5194/cp-9-621-2013, 2013.

758 Svendsen, J. I., Alexanderson, H., Astakhov, V. I., Demidov, I., Dowdeswell, J. A., Funder,
759 S., Gataullin, V., Henriksen, M., Hjort, C., Houmark-Nielsen, M., Hubberten, H. W.,
760 Ingolfsson, O., Jakobsson, M., Kjær, K. H., Larsen, E., Lokrantz, H., Lunkka, J. P., Lysså, A.,
761 Mangerud, J., Matiouchkov, A., Murray, A., Möller, P., Niessen, F., Nikolskaya, O., Polyak,
762 L., Saarnisto, M., Siegert, C., Siegert, M. J., Spielhagen, R., and Stein, R.: Late Quaternary
763 ice sheet history of northern Eurasia, Quat. Sci. Rev., 23, 1229-1271,
764 doi:10.1016/j.quascirev.2003.12.008, 2004.

765 Svendsen, J. I., Astakhov, V. I., Bolshiyanov, D. Y., Demidov, I., Dowdeswell, J. A.,
766 Gataullin, V., Hjort, C., Hubberten, H. W., Larsen, E., Mangerud, J., Melles, M., Möller, P.,
767 Saarnisto, M., and Siegert, M. J.: Maximum extent of the Eurasian ice sheets in the Barents
768 and Kara Sea region during the Weichselian, Boreas, 28, 234-242, doi:10.1111/j.1502-
769 3885.1999.tb00217.x, 1999.

770 Swingedouw, D., Fichefet, T., Huybrechts, P., Goosse, H., Driesschaert, E., and Loutre, M.
771 F.: Antarctic ice-sheet melting provides negative feedbacks on future climate warming,
772 Geophys. Res. Lett., 35, L17705, doi:10.1029/2008GL034410, 2008.

773 Turney, C. S. M., and Jones, R. T.: Does the Agulhas Current amplify global temperatures
774 during super-interglacials?, J. Quat. Sci., 25, 839-843, doi:10.1002/jqs.1423, 2010.

775 van de Berg, W. J., van den Broeke, M. R., van Meijgaard, E., and Kaspar, F.: Importance of
776 precipitation seasonality for the interpretation of Eemian ice core isotope records from
777 Greenland, Clim. Past., 9, 1589-1600, doi:10.5194/cp-9-1589-2013, 2013.

778 Zweck, C., and Huybrechts, P.: Modeling the marine extent of northern hemisphere ice sheets
779 during the last glacial cycle, Ann. Glaciol., 37, 173-180, 2003.

780 Zweck, C., and Huybrechts, P.: Modeling of the northern hemisphere ice sheets during the
781 last glacial cycle and glaciological sensitivity, J. Geophys. Res, 110, D07103,
782 doi:10.1029/2004JD005489, 2005.

783

784

785

11 Tables

Table 1: Matrix of all experiments and the respective ice sheet components that evolve in time (yes) or are fixed (no). In the latter case, freshwater fluxes (FWF, grey) are kept constant and topography and surface albedo are fixed to the preindustrial configuration.

EXP	topo NH	FWF NH	topo GrIS	FWF GrIS	topo AIS	FWF AIS
Reference	yes	yes	yes	yes	yes	yes
noGfwf	yes	yes	yes	no	yes	yes
noAGfwf	yes	yes	yes	no	yes	no
noAG	yes	yes	no	no	no	no
noIS	no	no	no	no	no	no

12 Figures

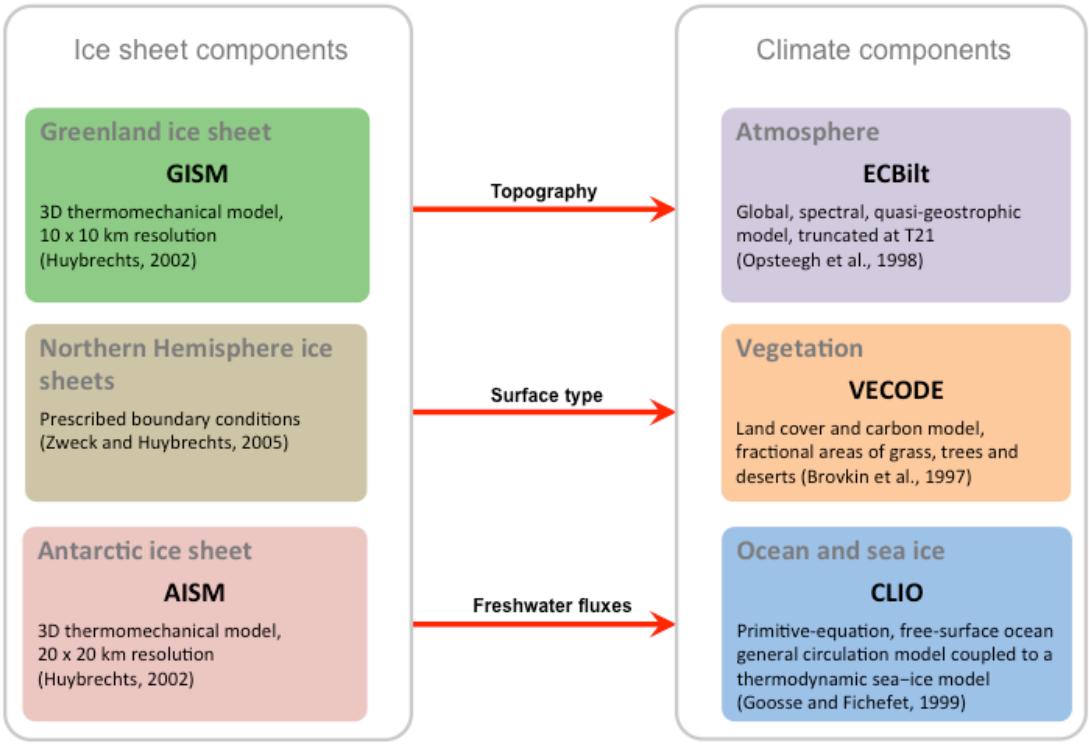

Figure 1: LOVECLIM model setup for the present study including prescribed ice sheet boundary conditions from the Northern Hemisphere, Greenland and Antarctic ice sheets.

797

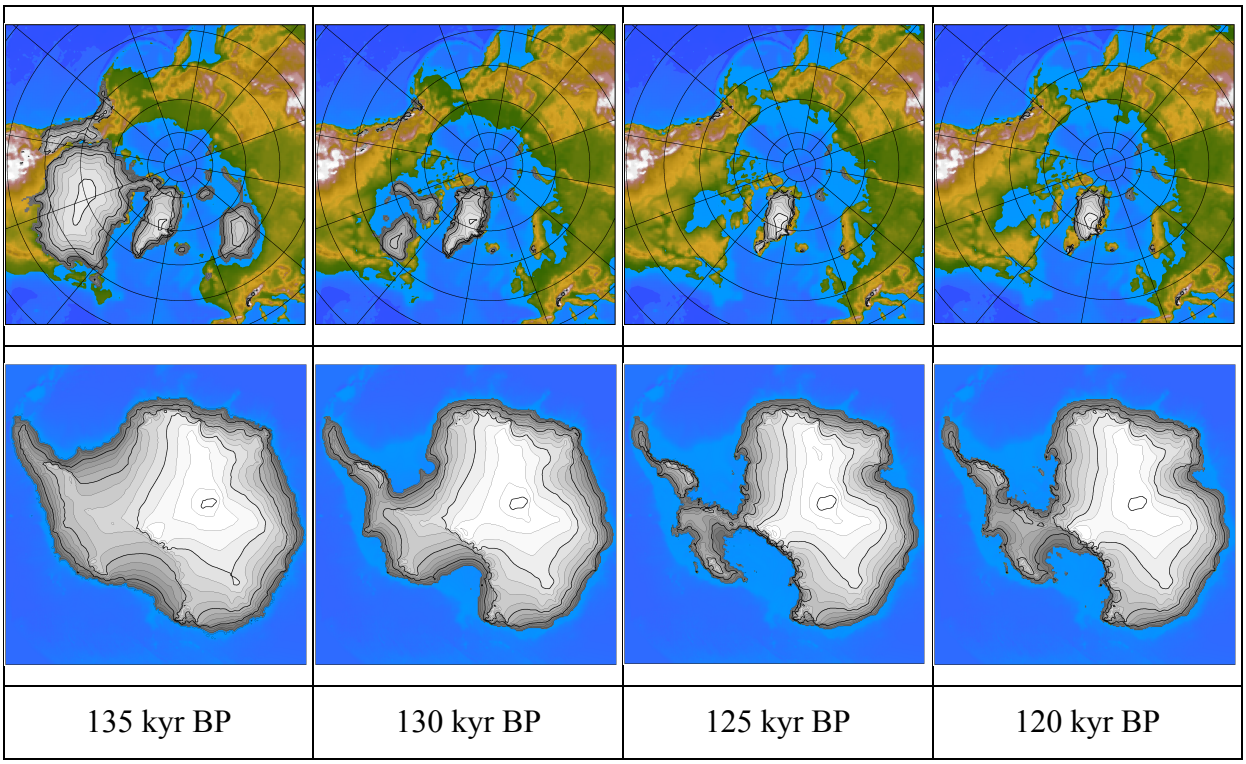

798 **Figure 2: Evolution of reconstructed Northern Hemisphere ice sheets and embedded modelled GrIS (top)**
799 **and modelled AIS (bottom) used as boundary conditions for the climate model.**

800

801

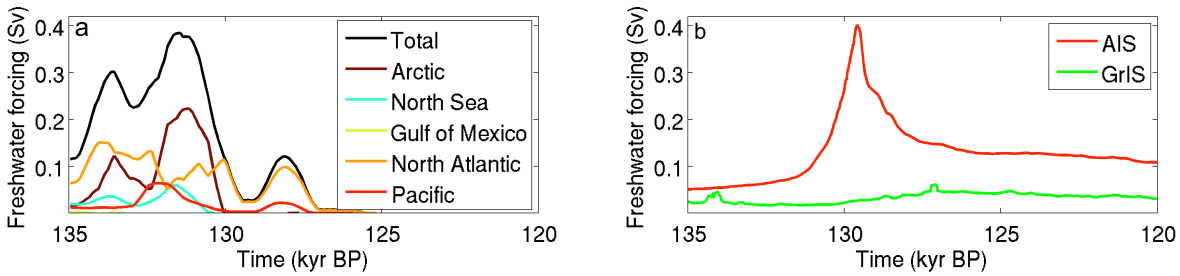

802 **Figure 3: Reconstructed freshwater forcing from the NH ice sheets (a) and from the GrIS and AIS (b). See**
803 **Goelzer et al. (2012) for definition of oceanic basins.**

804

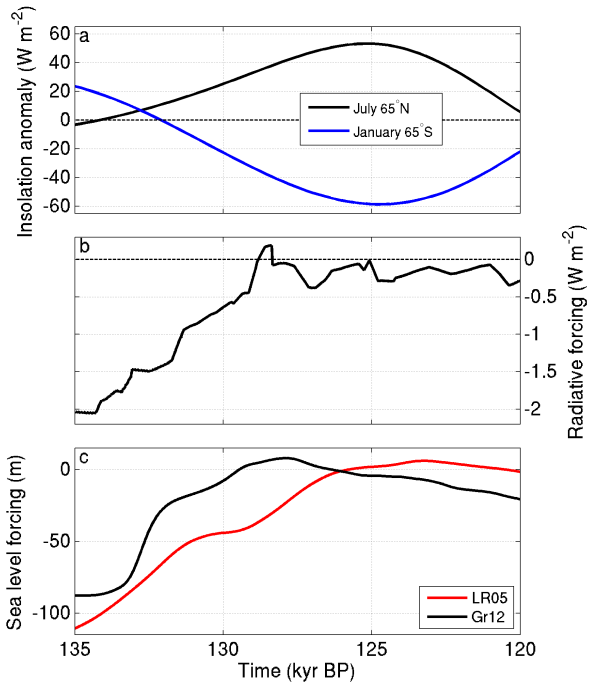

805 **Figure 4: Prescribed model forcings. (a) Average monthly insolation anomaly relative to the pre-industrial**
806 **at 65° North in July (black) and 65° South in January (blue). (b) combined radiative forcing anomaly of**
807 **prescribed greenhouse gas concentrations (CO_2, CH_4, N_2O) relative to the pre-industrial. (c) sea-level**
808 **forcing for the ice sheet components derived from either oceanic $\delta^{18}O$ data (Lisiecki and Raymo, 2005,**
809 **red) scaled to a global sea-level contrast between LGM and present day of 130 m or derived from a Red**
810 **Sea relative sea-level record (Grant et al. 2012, black).**
811

812

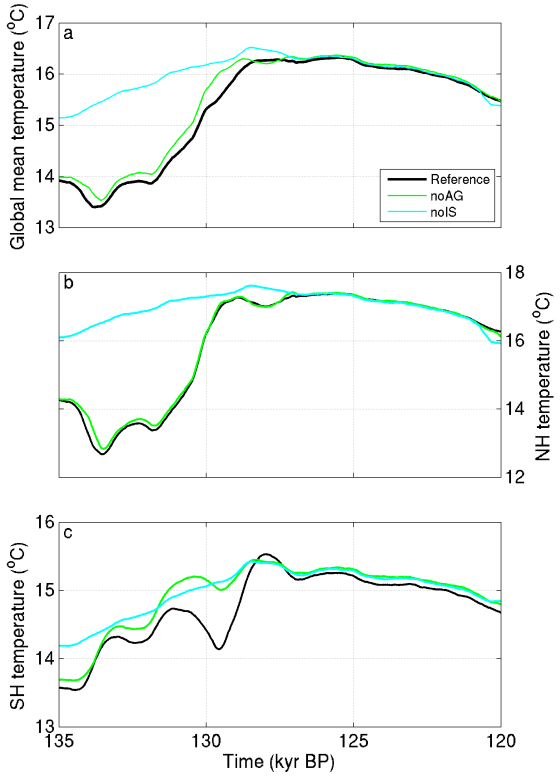

813 **Figure 5: Evolution of global mean (a), northern (b) and southern (c) hemispheric mean surface**
814 **temperature for experiments with different ice sheet forcing included. Curves are smoothed with a**
815 **running mean of 200 years for better comparison.**
816

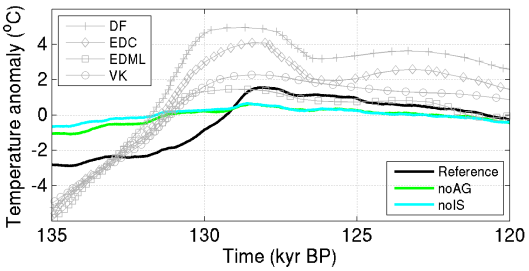

Figure 6: Comparison of modelled East Antarctic temperature evolution with reconstructed temperature changes at deep ice core sites. Modelled temperature anomalies are averaged over a region 72° - 90° S and 0° - 150° E. Ice core temperature reconstructions for the sites EPICA Dronning Maud Land (EDML, 75°00′ S, 00°04′ E), Dome Fuji (DF, 77°19′ S, 39°40′ E), Vostok (VK, 78°28′ S, 106°48′ E) and EPICA Dome C (EDC, 75°06′ S, 123°21′ E) are from Masson-Delmotte et al. (2011).

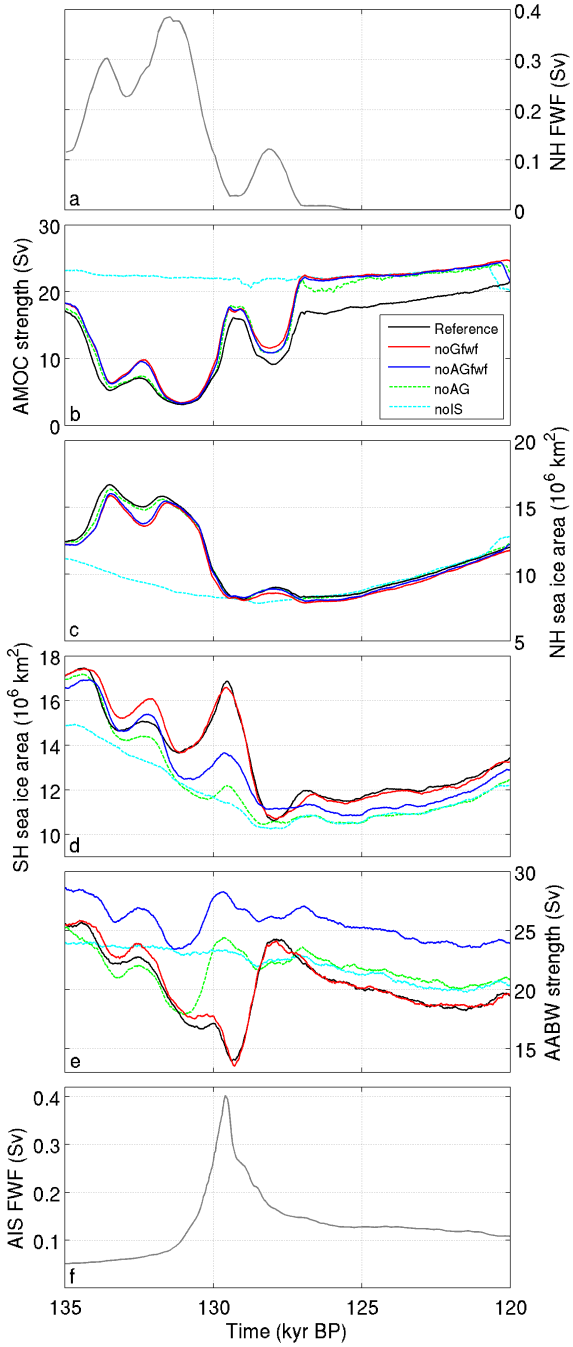

823 **Figure 7: Freshwater forcing and oceanic response characteristics. NH (a) and Antarctic ice sheet**
824 **freshwater fluxes (f), strength of the AMOC (b), NH sea ice area (c), SH sea ice area (d) and strength of**
825 **AABW formation (e) for the different experiments with and without freshwater forcing from Greenland,**
826 **Antarctic and NH ice sheet melting. Curves are smoothed with a running mean of 200 years for better**
827 **comparison.**
828

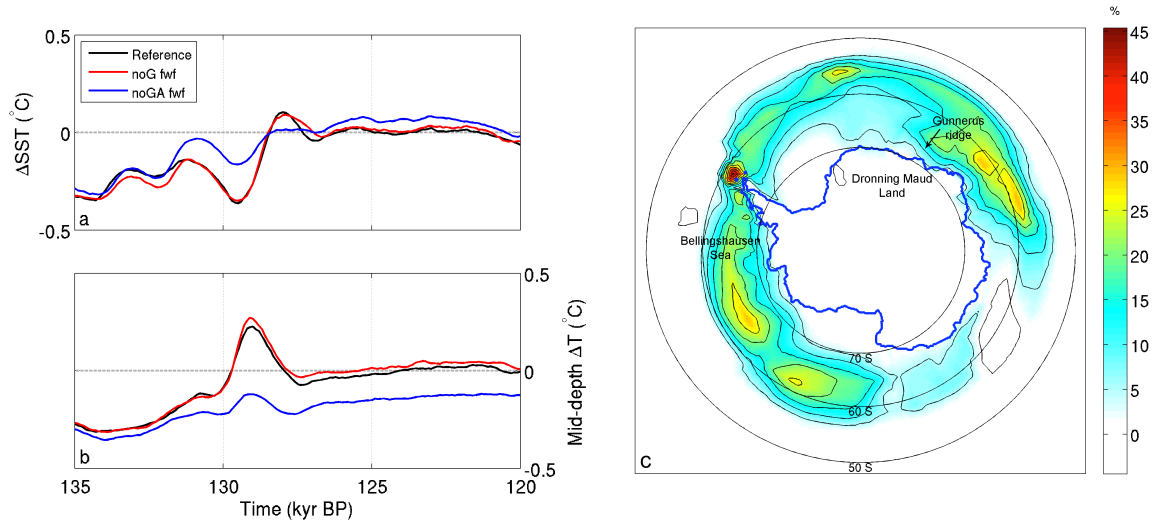

Figure 8: Evolution of annual mean sea surface temperature (a) and mid-depth (485-700 m) ocean temperature (b) anomalies relative to the pre-industrial in close proximity to the AIS (south of 63°S). (c) Meltwater related changes in annual mean sea ice area at 129.5 kyr BP from differences between experiments Reference and noAGfwf in per cent. The blue contour outlines the observed ice-shelf edge and grounded ice margin of the present-day AIS for illustration. All curves (a, b) are smoothed with a running mean of 200 years for better comparison.

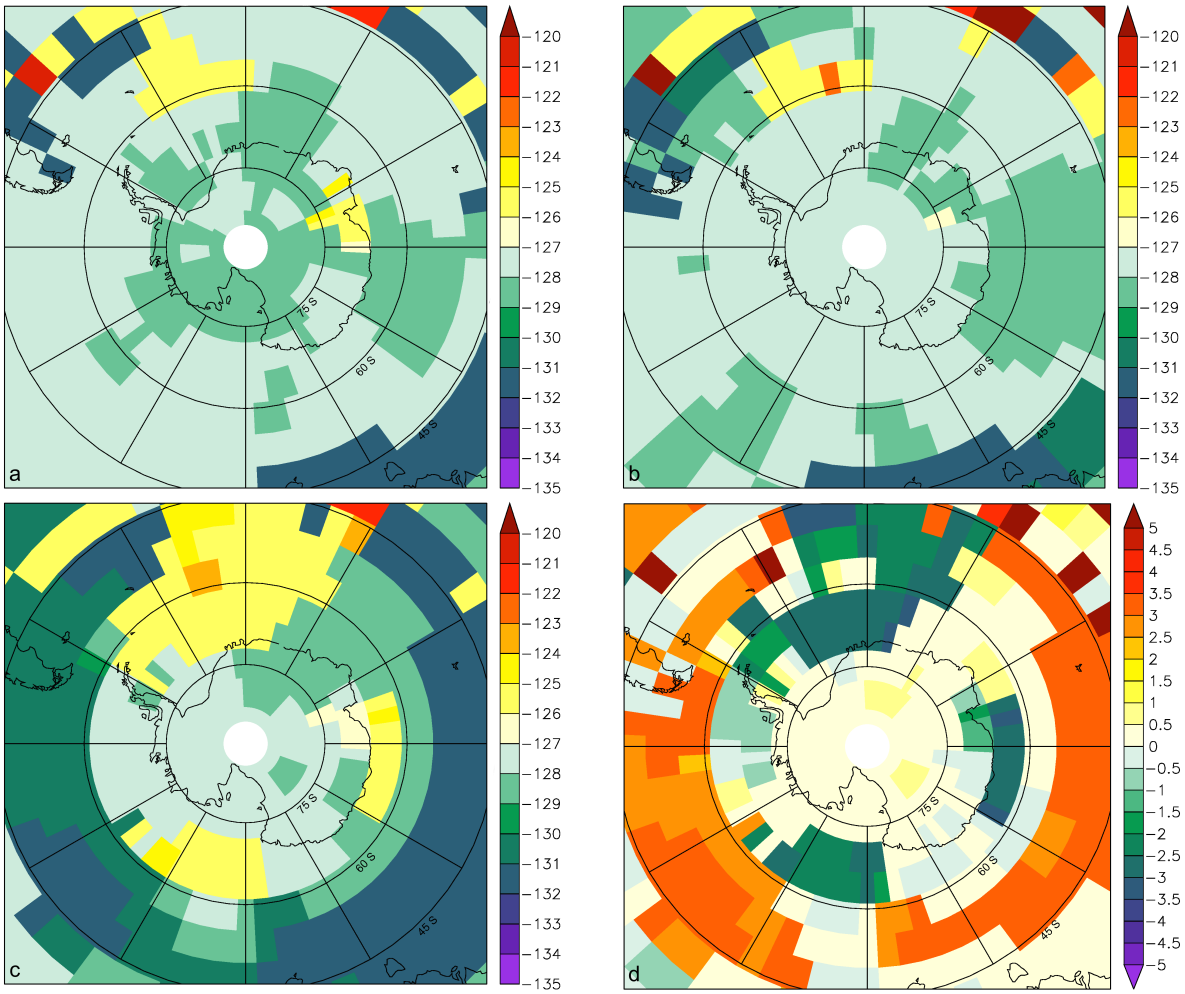

Figure 9: Time of maximum surface air temperature (MWT) in kyr BP for experiments Reference (a), noGfwf (b) and noAGfwf (c) and difference in MWT between experiments noGfwf and noAGfwf (d) in kyr, showing the shift of the MWT when Antarctic freshwater fluxes are included.

843 **Table A1: Sources of geomorphological data or modelling results used to prescribe changes in northern**
844 **hemisphere ice sheet extent for the post-LGM retreat.**

Ice Sheet	Source	Isochrone Time Period (kyr BP)
Laurentide	Dyke and Prest (1987)	18 – Present Day
Innuitian	Dyke et al. (2002)	18
Cordilleran	Clague and James (2001) Dyke et al. (2002) Mayewski et al. (1981)	20 – Present Day (south) 18 (north) 21 – 7 (interior)
Iceland	Andersen (1981)	20 – Present Day
Eurasian	Andersen (1981) Landvik et al. (1998) Mangerud et al. (2002) Svendsen et al. (1999)	20 – Present Day 15 – 12 (Barents Sea) 18 (Southern Barents and Kara Seas) 18
European Alps	Zweck and Huybrechts (2002)	21 – Present Day (modelled ice extent)

845

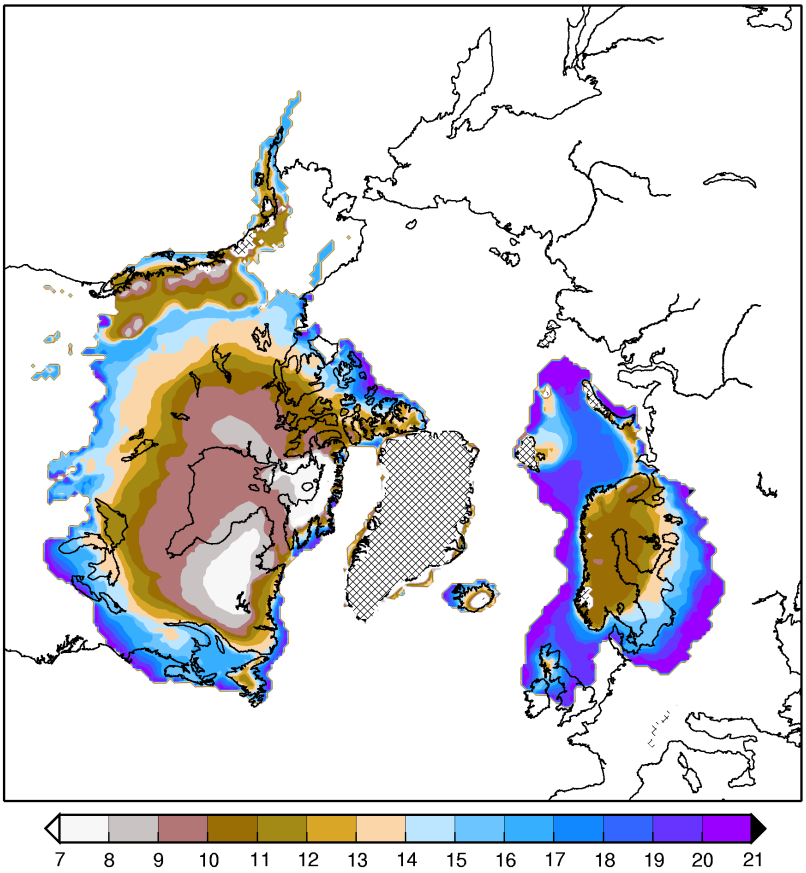

Figure A1: Interpolated ice sheet extent during the last deglaciation for the northern hemisphere ice sheets as a function of time (kyr BP). Hatched regions indicate present day ice.